

Coexistence of orbital degeneracy lifting and superconductivity in iron-based superconductors

H. Miao¹, L. -M. Wang², P. Richard¹, S. -F. Wu¹, J. Ma¹, T. Qian¹, L. -Y. Xing¹, X. -
C. Wang¹, C. -Q. Jin¹, C. -P. Chou^{4,2}, Z. Wang³, W. Ku², and H. Ding^{1*}

¹*Beijing National Laboratory for Condensed Matter Physics, and Institute of Physics,
Chinese Academy of Sciences, Beijing 100190, China*

²*Condensed Matter Physics and Materials Science Department, Brookhaven National
Laboratory, Upton, New York 11973, USA*

³*Department of Physics, Boston College, Chestnut Hill, Massachusetts 02467, USA*

⁴*Beijing Computational Science Research Center, Beijing 100084, China*

In contrast to conventional superconducting (SC) materials, superconductivity in high-temperature superconductors (HTCs) usually emerges in the presence of other fluctuating orders with similar or higher energy scales¹⁻⁵, thus instigating debates over their relevance for the SC pairing mechanism. In iron-based superconductors (IBSCs), local orbital fluctuations have been proposed to be directly responsible for the structural phase transition^{6,7} and closely related to the observed giant magnetic anisotropy and electronic nematicity⁸⁻¹². However, whether superconductivity can emerge from, or even coexist with orbital fluctuations, remains unclear. Here we report the angle-resolved photoemission spectroscopy (ARPES) observation of the lifting of symmetry-protected band

degeneracy, and consequently the breakdown of local tetragonal symmetry in the SC state of $\text{Li}(\text{Fe}_{1-x}\text{Co}_x)\text{As}$. Supported by theoretical simulations, we analyse the doping and temperature dependences of this band-splitting and demonstrate an intimate connection between ferro-orbital correlations and superconductivity.

In IBSCs, the orbital degree of freedom is believed to play an important role and can be closely related to the emergence of superconductivity^{13,14}. Ferro-orbital (FO) order, which leads to unequal occupation of d_{xz}/d_{yz} orbitals, has also been proposed as the origin of electronic nematicity^{6,7}. However, probing FO fluctuations directly in the absence of structural and magnetic phase transitions has never been explored, and whether FO fluctuations coexist or compete with the SC order is still an open question. In the tetragonal phase without spin-orbital coupling (SOC), d_{xz}/d_{yz} orbitals are degenerate at the Brillouin zone centre (Γ point), which is guaranteed by point-group symmetry. The formation of FO ordering would lift the degeneracy at Γ , resulting in a band gap Δ_{band} that can be monitored directly by ARPES.

In addition of having a natural non-polar cleaving surface preserving its bulk properties¹⁵⁻¹⁷, $\text{Li}(\text{Fe}_{1-x}\text{Co}_x)\text{As}$ has neither structural nor magnetic phase transitions in its whole phase diagram¹⁸, enabling us to study fluctuations in absence of long-range order. In Fig. 1, we compare the electronic band dispersion of LiFeAs and $\text{LiFe}_{0.88}\text{Co}_{0.12}\text{As}$ around the Γ point. Our polarization analysis confirms that the α and α' bands, which are mainly composed of d_{xz}/d_{yz} orbitals, have even and odd symmetries, respectively^{19,28,29}. The extracted band dispersion²⁰ in $\text{LiFe}_{0.88}\text{Co}_{0.12}\text{As}$ ($T_c = 4$ K) indicates that both the α and α' bands sink below E_F and are exactly

degenerate at the Γ point, as required by symmetry. In contrast, the α' band crosses E_F at $k_F = 0.03 \pi/a$ in the parent compound LiFeAs ($T_c = 18$ K), whereas the top of the α band lies about 12 meV below E_F , which means that the d_{xz}/d_{yz} orbitals are split in LiFeAs without long-range magnetic and orbital orders. To precisely resolve the band splitting, we recorded very high-energy resolution ARPES intensity plots of LiFeAs and LiFe_{0.88}Co_{0.12}As, as shown in Fig. 1. From the high-resolution data, we evaluate the band gap to $\Delta_{\text{band}} \sim 14$ meV in LiFeAs by extrapolating the top of the α' band using a parabolic fit, and we confirm the degeneracy of the d_{xz}/d_{yz} bands in LiFe_{0.88}Co_{0.12}As. By zooming near E_F , we find that the α' band further splits into two branches, as shown in Figs. 1c and 1g. While one branch is the continuous extension of the high binding energy dispersion, the other one shows an inflection point at 14 meV binding energy. As discussed later, the observed fine structure is consistent with the calculated electronic structure in the orbital nematic phase on twinned samples²¹, and supports that the observed band splitting is caused by FO fluctuations. As reported previously²², we distinguish an electron band at the Γ point of electron-doped LiFe_{0.88}Co_{0.12}As, which is not clear in the synchrotron-based results most likely due to different k_z positions. We suspect that this small electron band has a strong As p_z orbital component and is similar to the one observed in (Tl,Rb)_yFe_{2-x}Se₂²³.

To check whether the d_{xz}/d_{yz} splitting is a general feature of the IBSCs, we performed similar experiments on various materials and summarized the results in Fig. 2. We first considered LiFe_{0.94}Co_{0.06}As ($T_c = 10$ K), which has an intermediate doping between LiFeAs and LiFe_{0.88}Co_{0.12}As²⁹. Unlike in LiFeAs and similarly to LiFe_{0.88}Co_{0.12}As, the α' band falls below E_F . For this material, we find $\Delta_{\text{band}} = 10$

meV, suggesting that the band splitting is gradually suppressed as T_c decreases from 18 K to 4 K. We also studied the band splitting in $\text{NaFe}_{0.95}\text{Co}_{0.05}\text{As}$ ($T_c = 18$ K)²⁴, which is isostructural to LiFeAs (so-called 111 structure). From the extracted band dispersions displayed in Fig. 2d, we deduce that $\Delta_{\text{band}} = 15$ meV in this particular compound. Interestingly, all our data on the 111 crystal structure indicate that Δ_{band} scales with T_c in this family of materials, suggesting that the band splitting might be related to superconductivity. Interestingly, there is at least one other IBSC for which a d_{xz}/d_{yz} band splitting is clearly observed. Indeed, this observation has been reported for the $\text{FeTe}_{1-x}\text{Se}_x$ family of IBSCs^{25,26}. Using the data from Miao *et al.*²⁵, reproduced in Fig. 2e, we find that $\Delta_{\text{band}} = 18$ meV in $\text{FeTe}_{0.55}\text{Se}_{0.45}$, which is even larger than in LiFeAs . The observed band splitting in all the IBSCs studied here strongly suggests that the d_{xz}/d_{yz} separation at the Γ point has a fundamental origin.

We now focus on the temperature evolution of Δ_{band} in LiFeAs . For this purpose, we show in Fig. 3 high energy resolution ARPES cuts across the Γ point recorded between 50 and 250 K. The data are divided by the Fermi-Dirac function convoluted by the resolution function to reveal the band dispersion above E_F , which are obtained from parabolic fits. While the line width of the α and β bands broaden with temperature, their dispersions are unaffected. The α' band, on the other hand, gradually shifts downward and its top almost merges with that of the α band at 250 K. In Fig. 2m, we show the evolution of Δ_{band} as function of temperature by using different methods that all show that the d_{xz}/d_{yz} splitting decreasing gradually from nearly 0 at 250 K to about 14 meV at 50 K²⁹. Interestingly, the splitting survives even below the SC phase transition at 18 K. As shown in Figs. 2n - 2p, the α' band opens

up a SC gap below T_c , whereas the α band is barely changed. This observation proves that the band splitting coexists with superconductivity.

The observation of the degeneracy lifting of d_{xz}/d_{yz} orbitals in the tetragonal phase is puzzling. In order to demonstrate its origin, we investigate a simple model of quasi-1D electronic system (since d_{xz}/d_{yz} orbitals have strongly anisotropic quasi-1D hopping integral) under the influence of a spatially fluctuating local FO order parameter (represented by a diagonal Ising field)^{28,29}, and we display the results in Fig. 4. When the local order parameter has only short-range correlations (exponential decay), no clear indication of the fluctuating order is observed in the electronic structure other than the scattering of the particle that broadens the spectral function, as illustrated in the top row of Fig. 4. In contrast, when the spatial correlations of the local order parameter are long-ranged (power law decay), the quasiparticle peak splits in two and a pseudogap in the spectral function develops in between, as shown in Figs. 4f – 4h. This pseudogap corresponds to the splitting of the degenerate bands shown in Fig. 1. Although the spectral function exhibits features identical to those expected in the presence of a macroscopic long-range order, we emphasize that the system has not yet developed a true order, but only long-range spatial correlations. In other words, the one-particle Green's function has gone ahead and reflects the underlying “almost ordered” electronic structure. Therefore, the experimentally observed doping-dependent splitting between the d_{xz}/d_{yz} bands in the absence of FO order can be attributed to strong, slow-decaying, long-range FO correlations that cover a large region of the phase diagram and eventually support superconductivity at low temperature.

Very recently, an electronic Raman scattering study of $\text{Ba}(\text{Fe}_{1-x}\text{Co}_x)_2\text{As}_2$ ²⁷ and a combined study of magnetic-torque and X-ray in $\text{BaFe}_2(\text{As}_{1-x}\text{P}_x)_2$ ¹⁰ reported electronic nematicity in the absence of a magnetic phase transition. The observed “nematic” signal persists far above the SC and structural phase transitions, indicating the presence of a strong fluctuating orbital order, which is consistent with our doping- and temperature-dependent results. In the present study, we find that superconductivity emerges in the regime of strong FO correlations and that the SC transition temperature scales with the strength of the local orbital order, suggesting an intimate connection between FO correlations and superconductivity. This observation is very important since a recent ARPES and NMR study reports enhancement of low-energy antiferromagnetic spin fluctuations in $\text{LiFe}_{1-x}\text{Co}_x\text{As}$ samples with lower T_c ²², thus suggesting that such low-energy antiferromagnetic fluctuations alone do not control the strength of superconductivity in $\text{LiFe}_{1-x}\text{Co}_x\text{As}$.

Finally, we discuss the effect of spin-orbital coupling (SOC). In principle, SOC can lift the degeneracy of the d_{xz}/d_{yz} orbitals at the Γ point while maintaining local tetragonal symmetry. However, since SOC is a local effect and barely changes with doping and temperature, our observation of Δ_{band} variations as a function of doping and temperature is inconsistent with this scenario. Moreover, the clearly resolved inflection point on one branch of the fine structure shown in Fig. 1c is consistent with the calculated electronic structure in the orbital nematic phase on twinned samples²¹, and therefore supports our assumption that the observed d_{xz}/d_{yz} splitting is caused by FO fluctuations instead of SOC. Although spin fluctuations have been widely studied and discussed, fewer experimental studies on the orbital fluctuations can be found in the literature. Our study provides evidence of strong, long-range FO correlations in

IBSCs and demonstrates their intimate connection with superconductivity in $\text{LiFe}_{1-x}\text{Co}_x\text{As}$.

Methods:

Single crystals of $\text{LiFe}_{1-x}\text{Co}_x\text{As}$ were synthesized by a self-flux method using Li_3As , $\text{Fe}_{1-x}\text{Co}_x\text{As}$ and As powders as the starting materials. The Li_3As , $\text{Fe}_{1-x}\text{Co}_x\text{As}$ and As powders were weighed according to the element ratio of $\text{Li}(\text{Fe}_{1-x}\text{Co}_x)_{0.3}\text{As}$. The mixture was grounded and put into alumina crucible and sealed in Nb crucibles under 1 atm of Argon gas. The Nb crucible was then sealed in an evacuated quartz tube, heated to 1100 °C and slowly cooled down to 700 °C at a rate of 3 °C/hr. High energy resolution ARPES data were recorded at the Institute of Physics, Chinese Academy of Sciences, using the He I α ($h\nu = 21.2$ eV) resonance line of an helium discharge lamp. The angular and momentum resolutions were set to 0.2° and 3 meV, respectively. ARPES polarization measurements were performed at beamlines PGM and Apple-PGM of the Synchrotron Radiation Center (Wisconsin) equipped with a Scienta R4000 analyzer and a Scienta SES 200 analyzer, respectively. The energy and angular resolutions were set at 20 meV and 0.2°, respectively. All samples were cleaved *in situ* and measured in a vacuum better than 3×10^{-11} Torr.

Acknowledgement:

We thank A. Tsvelik, J.-P. Hu, F. Wang, P. D. Johnson and H.-B. Yang for useful discussions. This work was supported by grants from CAS (NO. 2010Y1JB6), MOST (Nos. 2010CB923000, 2011CBA001000, 2013CB921703), NSFC (11004232 and 11274362). Theoretical study is supported

by US Department of Energy, Office of Science DE-AC02-98CH10886. This work is based in part on research conducted at the Synchrotron Radiation Center, which is primarily funded by the University of Wisconsin-Madison with the University of Wisconsin-Milwaukee.

Author contributions:

H. M., T.Q., S.-F. W., and J. M. carried out the experiments; H. M. analyzed the data; L. -Y. X., X.-C. W. and C.-Q. J. provided samples; L.-M. W., C.-P. C., A.T and W. K. carried out the theoretical calculations; H. M., P. R., T. Q., L.-M. W., W. K. and H. D. wrote the paper. All authors discussed the results and commented on the manuscript.

Additional information:

The authors declare no competing financial interests.

Reference:

1. Aoki, D. *et al.* Coexistence of superconductivity and ferromagnetism in URhGe. *Nature* **413**, 613 (2001).
2. Tranquada, J. M. *et al.* Quantum magnetic excitations from stripes in copper oxide superconductors. *Nature* **429**, 534 (2004).
3. Tranquada, J. M. *et al.* Coexistence of, and competition between, superconductivity and charge-stripe order in $\text{La}_{1.6-x}\text{Nd}_{0.4}\text{Sr}_x\text{CuO}_4$. *Phys. Rev. Lett.* **78**, 338 (1997).
4. Pratt, D. K. *et al.* Coexistence of competing antiferromagnetic and superconducting phases in the underdoped $\text{Ba}(\text{Fe}_{0.953}\text{Co}_{0.047})_2\text{As}_2$ compound using x-ray and neutron scattering techniques. *Phys. Rev. Lett.* **103**, 087001 (2009).
5. Shermadini, Z. *et al.* Coexistence of magnetism and superconductivity in the iron-based compound $\text{Cs}_{0.8}(\text{FeSe}_{0.98})_2$. *Phys. Rev. Lett.* **106**, 117602 (2011).
6. Lee, C. –C, Yin, W. –G. & Ku, W. Orbital order and strong magnetic anisotropy in the parent compounds of iron-pnictide superconductors. *Phys. Rev. Lett.* **103**, 267001 (2009).
7. Lv, W. –C, Kruger, F & Phillips, P. Orbital ordering and unfrustrated $(\pi, 0)$ magnetism from degenerate double exchange in the iron pnictides. *Phys. Rev. B* **82**, 045125 (2010).
8. Chuang, T. –M. *et al.* Nematic electronic structure in “Parent” state of the iron-based superconductor $\text{Ca}(\text{Fe}_{1-x}\text{Co}_x)_2\text{As}_2$. *Science* **327**, 181 (2010).
9. Chu, J. –H. *et al.* In-plane resistivity anisotropy in an underdoped iron arsenide superconductor. *Science* **329**, 824 (2010).

10. Kasahara, S. *et al.* Electronic nematicity above the structural and superconducting transition in $\text{BaFe}_2(\text{As}_{1-x}\text{P}_x)_2$. *Nature* **486**, 382 (2012).
11. Yi, M. *et al.* Symmetry breaking orbital anisotropy observed for detwinned $\text{Ba}(\text{Fe}_{1-x}\text{Co}_x)_2\text{As}_2$ above the spin density wave transition. *Proc. Natl. Acad. Sci. USA* **108**, 6878 (2011).
12. Yi, M. *et al.* electronic reconstruction through the structural and magnetic transitions in detwinned NaFeAs . *New Journals of Physics* **14**, 073019 (2012).
13. Kontani, H. & Onari, S. Orbital-fluctuation-mediated superconductivity in iron pnictides: analysis of the five-orbital Hubbard-Holstein model. *Phys. Rev. Lett.* **104**, 157001 (2010).
14. Zhou, S., Kotliar, G. & Wang, Z. -Q. Extended Hubbard model of superconductivity driven by charge fluctuation in iron pnictides. *Phys. Rev. B* **84**, 140505(R) (2011).
15. Umezawa, K. *et al.* Unconventional anisotropic s-wave superconducting gaps of the LiFeAs iron-pnictide superconductors. *Phys. Rev. Lett.* **108**, 037002 (2012).
16. Borisenko, S. V. *et al.* Superconductivity without nesting in LiFeAs . *Phys. Rev. Lett.* **105**, 067002 (2010).
17. Allan, M. P. *et al.* Anisotropic energy gaps of iron-based superconductivity from intraband quasiparticle interference in LiFeAs . *Science* **336**, 563 (2012).
18. Wang, X. -C. *et al.* The superconductivity at 18 K in LiFeAs system. *Solid State Commun.* **148**, 538 (2008).
19. Wang, X. -P. *et al.* Orbital characters determined from Fermi surface intensity patterns using angle-resolved photoemission spectroscopy. *Phys. Rev. B* **85**, 214518 (2012).

20. Johnson, P. D. *et al.* Doping and temperature dependence of the mass enhancement observed in the cuprate $\text{Bi}_2\text{Sr}_2\text{CaCu}_2\text{O}_{8+\delta}$. *Phys. Rev. Lett.* **87**, 177007 (2001).
21. Liang, S.-H., Moreo, A. & Dagotto, E. Nematic state of pnictides stabilized by interplay between spin, orbital and lattice degree of freedom. *Phys. Rev. Lett.* **111**, 047004 (2013).
22. Ye, Z.-R. *et al.* Orbital selective correlations between nesting/scattering/Lifshitz transition and the superconductivity in $\text{AFe}_{1-x}\text{Co}_x\text{As}$ (A= Li, Na). Preprint at <http://arxiv.org/abs/1303.0682> (2013).
23. Liu, Z.-H. *et al.* Three dimensionality and orbital characters of the Fermi surface in $(\text{Tl,Rb})_y\text{Fe}_{2-x}\text{Se}_2$. *Phys. Rev. Lett.* **109**, 037003 (2012).
24. Liu, Z. -H. *et al.* Unconventional superconducting gap in $\text{NaFe}_{0.95}\text{Co}_{0.05}\text{As}$ observed by angle-resolved photoemission spectroscopy. *Phys. Rev. B* **84**, 064519 (2011).
25. Miao, H. *et al.* Isotropic superconducting gaps with enhanced pairing on electron Fermi surfaces in $\text{FeTe}_{0.55}\text{Se}_{0.45}$. *Phys. Rev. B* **85**, 094506 (2012).
26. Tan, S. -Y. *et al.* Interface-induced superconductivity and strain-dependent spin density waves in $\text{FeSe}/\text{SrTiO}_3$ thin films. *Nature Mater.* **12**, 634 (2013).
27. Gallais, Y. *et al.* Observation of incipient charge nematicity in $\text{Ba}(\text{Fe}_{1-x}\text{Co}_x)_2\text{As}_2$. Preprint at <http://arxiv.org/abs/1302.6255> (2013).
28. Chia-Hui Lin, Tom Berlijn, Limin Wang, Chi-Cheng Lee, Wei-Guo Yin, & Wei Ku, One-Fe versus Two-Fe Brillouin Zone of Fe-Based Superconductors: Creation of the Electron Pockets by Translational Symmetry Breaking, *Phys. Rev. Lett.* **107**, 257001 (2011).
29. Supplement materials.

Figure 1 | Observation of split d_{xz}/d_{yz} bands in LiFeAs and degenerate d_{xz}/d_{yz} bands in $\text{LiFe}_{0.88}\text{Co}_{0.12}\text{As}$. **a** and **e**, ARPES intensity plots of LiFeAs measured along the Γ -M direction, and recorded with 51 eV incident light in the σ and π configurations to select odd and even orbital symmetries^{19,28,29}, respectively. **b** and **f**, Same as panels **a** and **e**, but for $\text{LiFe}_{0.88}\text{Co}_{0.12}\text{As}$. **c** and **d**, High energy resolution ARPES cuts along the Γ -M direction of LiFeAs and $\text{LiFe}_{0.88}\text{Co}_{0.12}\text{As}$, respectively, recorded with the He I α line of an helium discharge lamp. The red and blue curves in panel **a**, **b**, **e** and **f** are the original and fitted momentum distribution curves at E_F , respectively. The red, blue and green circles represent the peak positions associated with the α (d_{even}), α' (d_{odd}) and β (d_{xy}) bands, respectively, where d_{odd} (d_{even}) is the odd(even) linear combination of the d_{xz} and d_{yz} orbitals. By comparing the extracted band dispersions, we conclude that the band top of the d_{xz}/d_{yz} bands are split in LiFeAs and degenerate in $\text{LiFe}_{0.88}\text{Co}_{0.12}\text{As}$. The zoom on the high energy resolution data of **c** reveals that the α' band is further split into two branches, as shown in the inset. **g** and **h**, EDCs corresponding to the data shown in panels **c** and **d**, respectively. The blue EDC in panel **g**, also shown in inset, illustrates the splitting of the α' band.

Figure 2 | Doping and material dependence of the d_{xz}/d_{yz} band splitting. a

– **c**, Extracted band dispersion of the d_{xz}/d_{yz} bands in LiFeAs, LiFe_{0.94}Co_{0.06}As²⁹, and LiFe_{0.88}Co_{0.12}As, respectively. **d** and **e**, Extracted band dispersion of NaFe_{0.95}Co_{0.05}As²⁴ and FeTe_{0.55}Se_{0.45}²⁵, respectively. Red dashed curves are parabolic fits. **f**, Doping and T_c dependence of Δ_{band} . The open and plain symbols refer to the doping (bottom) and T_c (top) axes. Error bars are determined by standard deviation of the fitting parameters²⁹.

Figure 3 | Temperature evolution of the band gap Δ_{band} and its coexistence with superconductivity. **a – e**, High energy resolution ARPES intensity plots at $T = 250$ K, 200 K, 150 K, 100 K and 50 K, respectively. **f – j**, Same data but divided by the Fermi-Dirac function convoluted with the system resolution function to probe the electronic structure above E_F . Band dispersions at different temperatures are extracted using momentum distribution curves (MDCs) and fitted to parabolic functions. **k**, Energy distribution curves (EDCs) at the Γ point at different temperatures. We used two Lorentzian peaks to extract the top of the α and α' bands, and plot the fitted results on top of the original data using red dashed curves²⁹. The top of the α' band is shifted towards high binding energy as temperature increases, and it almost merges with the top of the α band at 250 K. **l**, MDCs recorded 20 meV below E_F , which corresponds to the red dashed lines shown in **a – e**. At high temperature, the α' peak positions move towards Γ , indicating that the band moves downward in energy. In contrast, the peak positions of the α and β bands are unchanged²⁹. **m**, temperature evolution of Δ_{band} . The values of Δ_{band} are extracted from the electronic band dispersions, EDCs and MDCs. Error bars are determined by the standard deviation of the fitted parameters. **n** and **o** are ARPES intensity plots just above and well below T_c , respectively. **p**, EDCs at the Γ point above and below T_c .

Figure 4 | Sensing long-range correlations without real order. In a typical mean-field treatment, the effects of the order parameter, for example a gap opening, are only visible in the presence of long-range order, represented by a non-zero order parameter. Without a real long-range order, the local order parameter only scatters the carriers and smears the spectral function. This is illustrated by the upper panels: **a**, an example of the configuration of a FO disordered system (represented by an Ising field) without long-range correlations, **b**, the resulting average band structure that couples to the Ising field, showing no clear splitting of the band. **c**, **d**, the average spectral function at momentum $\mathbf{k}=(0,0)$ and $\mathbf{k}=(0.25,0.25)$. However, the situation becomes interesting when the disordered system contains long-range, power-law decaying correlations of the local order parameter. The lower panels **e-h** illustrates this interesting FO disordered case. One finds that even though the order parameter remains zero, the average spectral function now demonstrates clear signatures of coupling to the local order. For example, a splitting of degeneracy is observed in **f**, and a pseudo-gap is found in **g**, both of which being expected in the presence of an order parameter, but now already occur in the disordered system with long-range correlations.

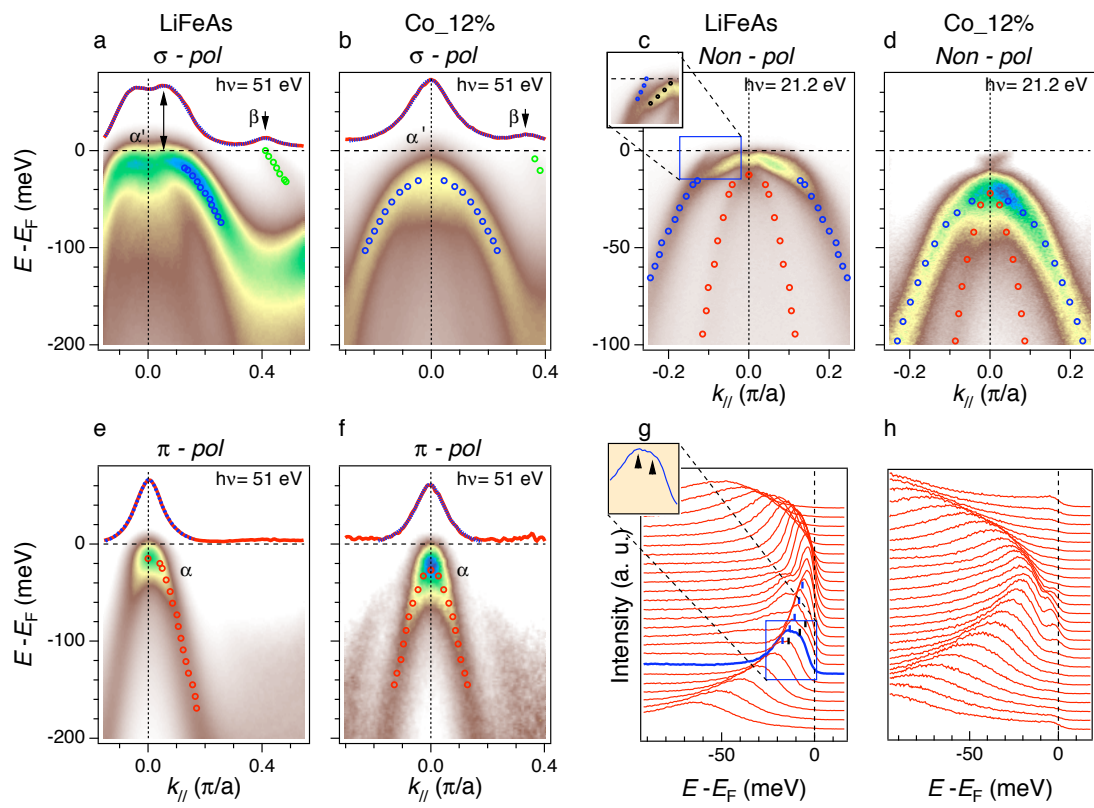


Figure 1

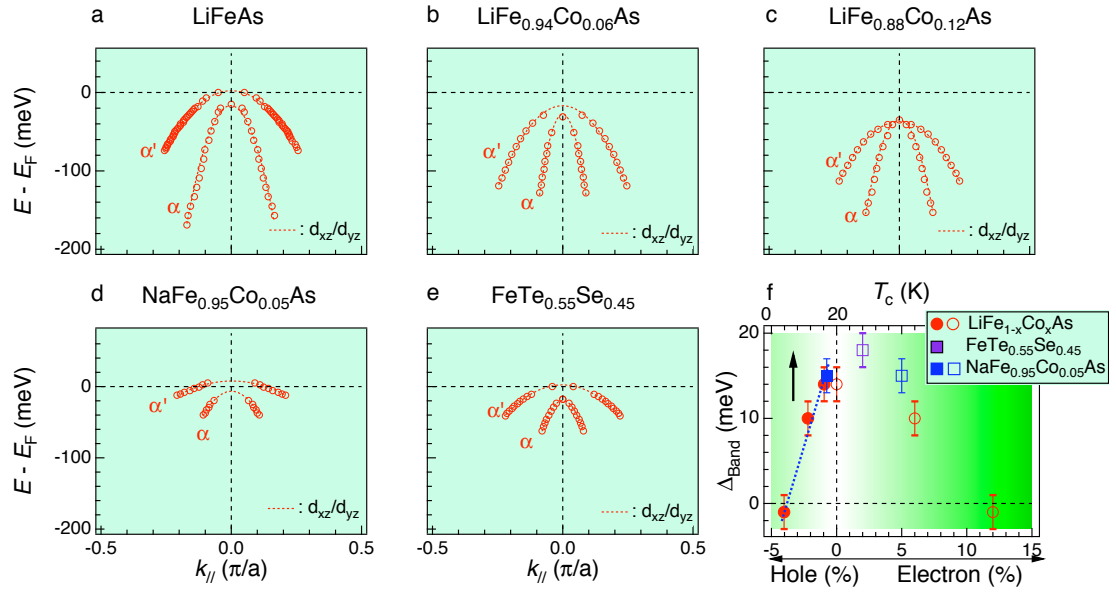


Figure 2

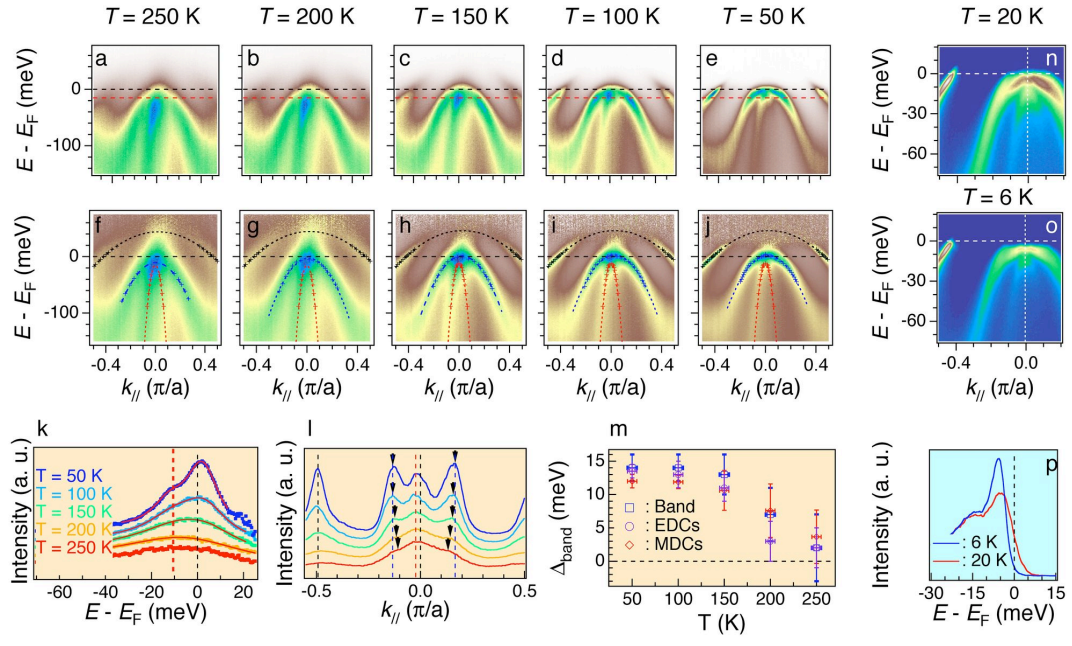


Figure 3

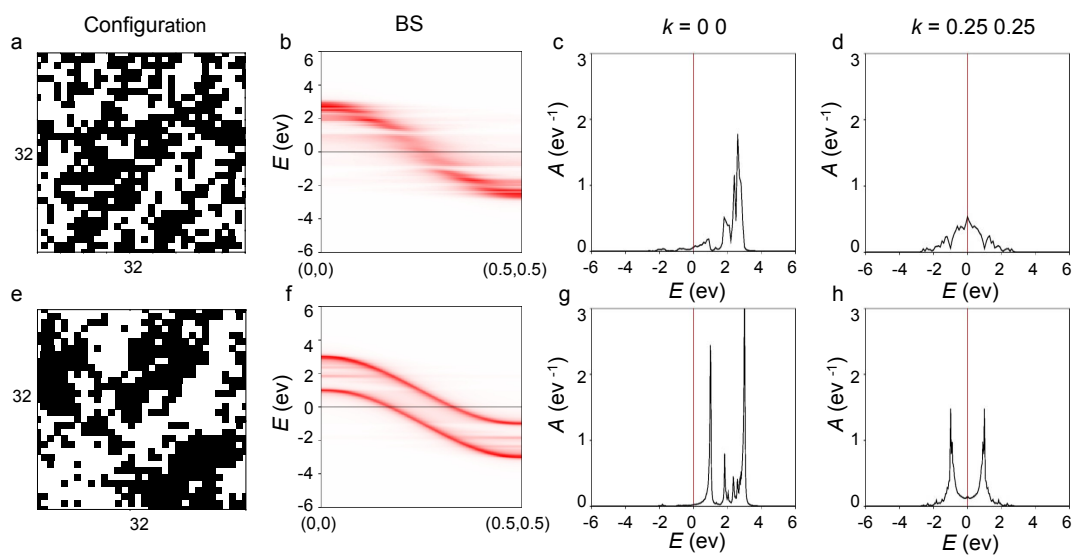


Figure 4